Available online at www.sciencedirect.com
ScienceDirect
Journal of Photochemistry and Photobiology A: Chemistry 188 (2007) 235–244
Journal of Photochemistry and Photobiology A:Chemistry
www.elsevier.com/locate/jphotochem

Experimental investigations by using electrochemical, steady state and time resolved spectroscopic tools on the photoreactions of disubstituted indoles in presence of tetracyanoquinodimethane (TCNQ) and a theoretical approach by using time-dependent density functional theory

Paulami Mandal, Tanushree Sahu [1], Tapas Misra, Suman K. Pal, Tapan Ganguly *

Department of Spectroscopy, Indian Association for the Cultivation of Science, Jadavpur, Kolkata 700032, India

Received 25 July 2006; received in revised form 11 November 2006; accepted 12 December 2006
Available online 16 December 2006

Abstract

The spectroscopic and photophysical properties of some dimethylindoles, 1,2-dimethylindole (12DMI) and 2,3-dimethylindole (23DMI) were measured in presence of electron acceptor, tetracyanoquinodimethane (TCNQ) in solvents of varying polarity by using electrochemical, steady state and time resolved spectroscopic techniques. Both from the theoretical considerations made by using time-dependent density functional theory (TD-DFT) and steady state polarization spectral measurements, it reveals the possibility of mixing of the two closely lying lowest electronic excited states ^1L_a (S2) and ^1L_b (S1) of DMIs. Though Stern–Volmer (SV) analysis of steady state measurements is unable to provide the information on the concurrent occurrences of static and dynamic processes involved, but electrochemical measurements coupled with time resolved spectroscopic investigations demonstrate that TCNQ may act as a potential electron acceptor in presence of dimethylindoles to undergo highly exergonic photoinduced electron transfer reactions in Marcus inverted region. Possibility of building up of various artificial or model photoactive systems with the linked DMI–TCNQ dyad systems is hinted at.

Keywords: Photoinduced electron transfer; Static quenching; Dynamic quenching; Transient absorption spectra; TD-DFT

1. Introduction

For better understandings of redox proteins [1–3], photophysical and photochemical studies on indoles still remain as a very active field of research [4–18]. As indoles are the chromophores of the amino acid tryptophan, investigations on indole derivatives are very much helpful in revealing the long range electron transfer (ET) mechanism in proteins. Our primary interest is to develop efficient photoconducting materials when well known organic π-electron acceptors would be sensitized by indole derivatives. Two main π-electron acceptors known are 9-cyanoanthracene (9CNA) and 7,7,8,8-tetracyanoquinodimethane (TCNQ). It was reported earlier that good charge transfer (CT) complex conductors are formed between good donor and acceptor pairs whose molecular shapes are flat [19]. Hence indole compounds along with 9CNA or TCNQ seem to be potential candidates to form photoconducting materials. In the present investigations we used disubstituted indoles rather than monosubstituted ones because we observed before [5] from electrochemical measurements that the electron donating capabilities of disubstituted indoles are larger. We already made systematic steady state and time resolved spectroscopic studies [5] on the photoinduced electron transfer reactions between some disubstituted indoles (DMIs) and 9CNA. It was found that in highly polar medium acetonitrile (ACN), the major non-radiative pathway seems to be due

* Corresponding author. Tel.: +91 33 2473 4971x253; fax: +91 33 2473 2805.
E-mail addresses: tapcla@rediffmail.com, sptg@mahendra.iacs.res.in (T. Ganguly).
[1] Present address: Department of Physics, Ramananda College, Bishnupur, West Bengal, India.

1010-6030/$ – see front matter © 2006 Elsevier B.V. All rights reserved.
doi:10.1016/j.jphotochem.2006.12.018

to photoinduced electron transfer (PET). Thus dynamic processes are mainly involved in quenching phenomena observed. In the present investigation, we observed combined mechanisms of quenching (static and dynamic) with TCNQ acceptors. Detailed studies were made by using electrochemical, steady state and time resolved (fluorescence lifetime and transient absorption) spectroscopic techniques to reveal the mechanisms of charge separation or electron transfer reactions within the disubstituted indoles 1,2-dimethylindole (12DMI) or 2,3-dimethylindole (23DMI) and well known electron acceptor TCNQ (Fig. 1a). All the results obtained from the present theoretical (TD-DFT) and experimental investigations seemingly indicate that TCNQ may be better candidate than 9CNA in building good photoconducting or solar energy conversion devices when linked with the DMIs. In the present paper the results and their interpretations are provided in details.

2. Experimental

2.1. Materials

All the samples 12DMI, 23DMI and TCNQ (97% pure), supplied by Aldrich, were purified by vacuum sublimation. The solvents *n*-haptane (NH), tetrahydrofuran (THF), acetonitrile (ACN) (SRL) and ethanol (EtOH) of spectroscopic grade were distilled under vacuum according to the standard procedure and tested before use for the presence of any impurity emission in wavelength region studied.

2.2. Spectroscopic apparatus

At the ambient temperature (296 K) steady state electronic absorption and fluorescence emission spectra of dilute solutions (10^{-4} to 10^{-6} mol dm^{-3}) of the samples were recorded using 1 cm path length rectangular quartz cells by means of an absorption spectrophotometer (Shimadzu UV-VIS 2401PC) and F-4500 fluorescence spectrophotometer (Hitachi), respectively. Fluorescence lifetime measurements were carried out using the Time Master fluorimeter from Photon Technology International (PTI). The system measures fluorescence lifetimes using PTI's patented strobe technique and gated detection. The software FeliX32 controls all acquisition modes and data analysis of the Time Master system. The sample was excited using a thyratron gated nitrogen flash lamp (width ~2 ns) capable of measuring fluorescence time resolved acquisitions at a flash rate of 25 kHz. Lamp profiles were measured at the excitation wavelength (297 nm or 337 nm) with a band pass of 3 nm or 1 nm, respectively having Ludoc as the scatterer. The quality of fit has been assessed over the entire decay, including the rising edge, and tested with a plot of weighted residuals, the other statistical parameters, e.g., the χ^2 and the Durbin–Waston (DW) parameters. All the solutions for room temperature measurements were deoxygenated by purging with argon gas stream for about 30 min.

The degree of polarization (P) was measured with the help of UV–vis polarizer accessories including UV Liner

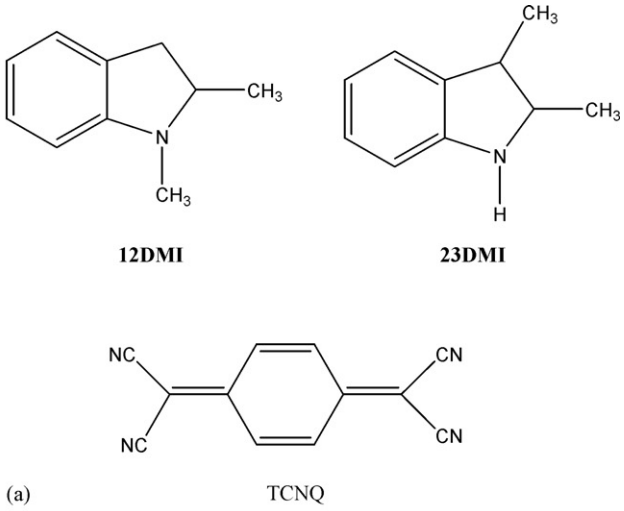

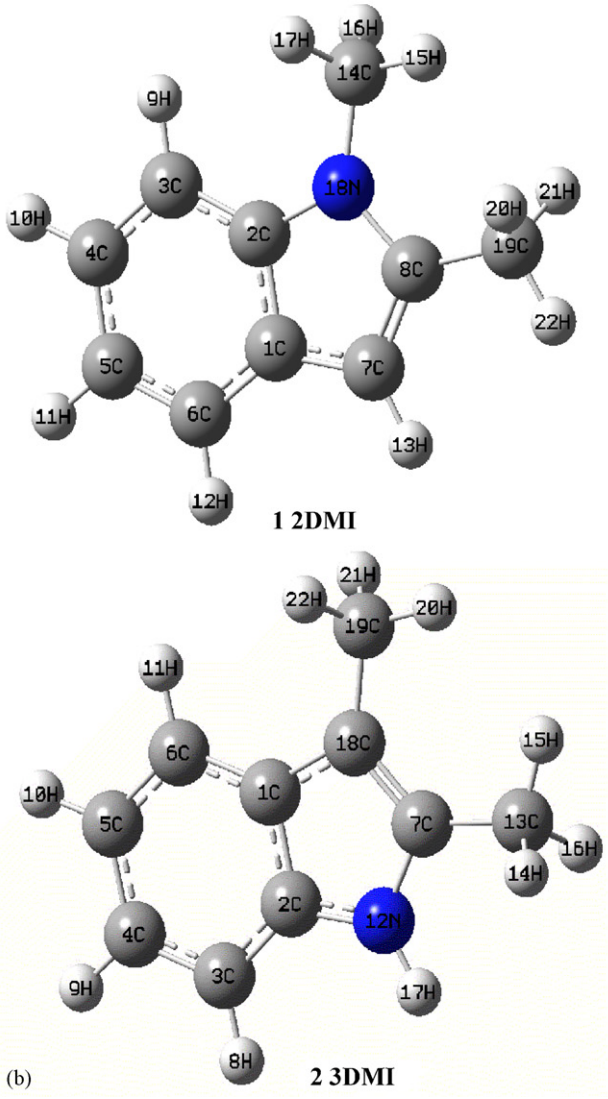

Fig. 1. (a) Molecular structures of 12DMI, 23DMI and TCNQ. (b) B3LYP/6-31G(d) optimized geometries of 12DMI and 23DMI.

Dichoric polarizer, wavelength range 230–770 nm, purchased from Oriel Instruments, USA. The observed degree of polarization (P) values were obtained from the following relation [20,21]:

$$P = \frac{I_{EE} - (I_{BE}/I_{BB})I_{EB}}{I_{EE} + (I_{BE}/I_{BB})I_{EB}} \quad (1)$$

Here, I_{EE} and I_{EB} are the intensities of parallel and perpendicular polarized emission with vertically polarized excitation and I_{BB} and I_{BE} are the intensities of horizontally and vertically polarized emission when excited with horizontally polarized light. I_{BE}/I_{BB} defines the instrumental correction factor G (polarization characteristic of the photometric system). This correction is made for any change in the sensitivity of the emission channel for the vertically and horizontally polarized components.

2.3. Laser flash photolysis

The third harmonic (355 nm) output pulses of 35 ps duration and energy ~6 mJ pulse^{-1} from an active–passive mode-locked Nd:YAG laser (Continuum model 501-C-10) were used for excitation of the samples. Transients were studied by monitoring their absorption using a tungsten filament lamp in contribution with a Bausch and Lomb monochromator (*f*/10, 350–800 nm), Hamamatsu R 928 PMT, and a 500 MHz digital storage oscilloscope (Tektronix, TDS-540A) connected to a PC.

2.4. Electrochemical measurements

Electrochemical measurements were made to determine the redox potentials of the reactants by using the PAR model VersaStat II electrochemistry system. Three electrode systems including Ag/AgCl as reference electrode were used in the measurements. Tetraethylammonium perchlorate (TEAP) in ACN was used as a supporting electrolyte.

2.5. Computational methods

The (gas phase) ground state geometry of 12DMI and 23DMI (Fig. 1) was fully optimized without symmetry constraints, using the B3LYP hybrid functional and the 6-31G(d,p) basis set. The gas phase vertical excitation energies using the optimized geometries for these molecules were computed by using the time-dependent DFT (TD-DFT) methods (using the B3LYP hybrid functional and 6-31G(d,p) basis set implemented in the Gaussian package) [21]. The effect of solvation on the computed TD-DFT vertical excitation energies was investigated by using a continuum solvation model, specifically, polarization continuum model (PCM) implemented for excited states. Because we are interested in vertical excitation energies, the PCM–TD-DFT calculations were carried out with non-equilibrium solvation conditions. All calculations were carried out with the Gaussian 98 and Gaussian 03 programs.

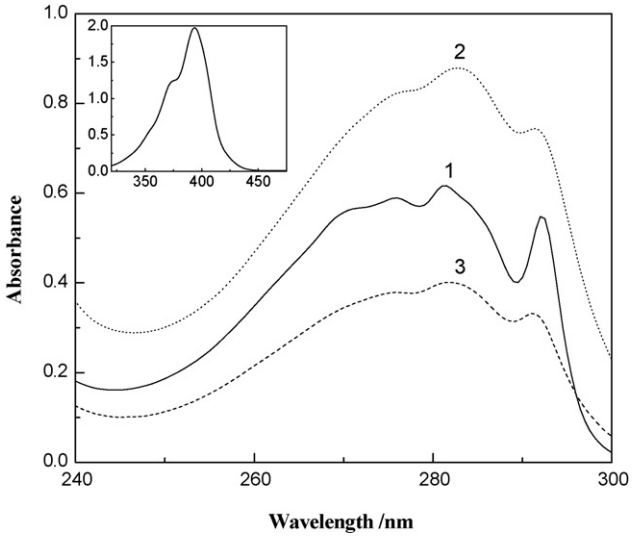

Fig. 2. Steady state electronic absorption spectra of 12DMI at the ambient temperature in (1) NH, (2) ACN, and (3) EtOH (inset: UV–vis absorption spectra of TCNQ at the ambient temperature).

3. Results and discussion

3.1. Spectroscopic investigations on 12DMI and 23DMI

3.1.1. UV–vis spectra of DMIs in the different polarity solvents at the ambient temperature

The UV–vis spectra of both 12DMI and 23DMI exhibit lower energy band systems in the region of 260–300 nm in solvents of different polarity (Fig. 2). Within the low energy band envelop observed in non-polar NH, a sharp (0, 0) band resides at 290 nm position and the band maximum situates at nearly 281 nm. With the increase of the polarity of the environment from NH to EtOH to ACN, the absorption band maximum (~281 nm) undergoes a small red shift whereas the (0, 0) band position at about 290 nm remains unaltered. As the energy position of the latter band remains unchanged with the polarity of the medium, this band system could be assigned to $^1L_b \leftarrow {}^1A$ transition because this type of transition is generally insensitive to the polarity of the environment. On the other hand the red shift of the band maximum at 281 nm indicates that the nature of the transition responsible for this band should be of $^1L_a \leftarrow {}^1A$ type which possesses charge transfer character.

Further, polarized fluorescence excitation spectra of both DMIs, measured in pure EtOH rigid glassy matrix at 77 K, clearly show (Fig. 3a) that the positive P value gradually decreases in magnitude from (0, 0) band position (mostly the region of ^1L_b) to the band maximum region where relatively ^1L_a transition dominates. This observation demonstrates that the fluorescence emission mainly originates from the lowest lying electronic state ^1L_b and the low energy absorption band system resided within 260–300 nm is responsible for the mixed states of ^1L_a and ^1L_b. As the phosphorescence lifetimes of both the DMIs are around 4 s, $T_1 \leftarrow S_0$ transition could logically be assigned to π–π^* nature. In organic molecular system, π–π^* type triplet–singlet (T_1–S_0) transition moment should be perpendicular to the molecular plane on which the ^1L_a and ^1L_b

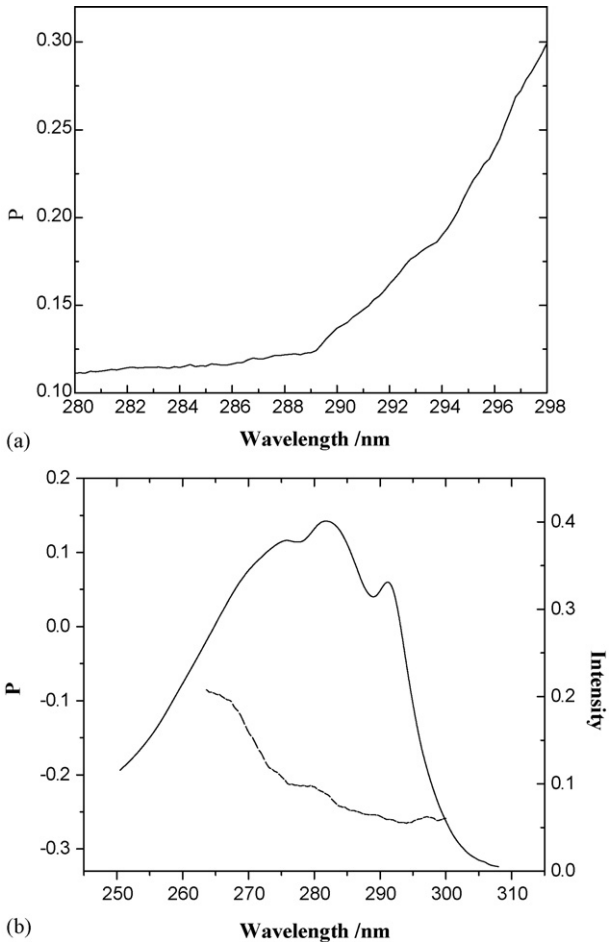

Fig. 3. (a) Fluorescence excitation polarization spectra of 12DMI (λ_{em} = 318 nm) in EtOH rigid glassy matrix at 77 K. (b) Solid line represents the fluorescence excitation spectra of 12DMI in EtOH rigid glassy matrix at 77 K, and the broken line shows the phosphorescence excitation polarization spectra (λ_{em} = 430 nm).

transitions, being in general orthogonal to each other as in carbazoles and other similar compounds, lie. This may be the reason for the observation of negative *P* values of varying magnitudes throughout the phosphorescence excitation spectra from 300 nm to 270 nm, i.e., from ^1L_b domain to the region of ^1L_a (Fig. 3b).

The measurement of polarized phosphorescence excitation spectra (Fig. 3b) also corroborates the views, made from the spectra of polarized fluorescence excitation, that the low energy absorption band of DMI (12 or 23) is mainly composed of the mixture of the two lowest lying electronic states, ^1L_a and ^1L_b.

3.1.1.1. Ground state calculations: molecular geometry, ground state dipole moments and transition dipoles. The B3LYP/6-31G(d,p) optimized ground state geometries for 12DMI and 23DMI are shown in Fig. 1b (Cartesian coordinates are provided in the supporting information). The TD-DFT theory predicts a nearly planar geometry of both the 12DMI and 23DMI.

The dihedral angle of 12DMI defined by 3C–2C–N–14C is predicted to be −1.5053° by TD-DFT theory and for 23DMI, 3C–2C–N–17H is 0.0167°. The ground state dipole moment of 12DMI and 23DMI predicted by density functional theory is 2.72 D and 2.42 D, respectively.

Molecular orbitals. The HOMO−1, HOMO, LUMO and LUMO+1 orbitals for 12DMI and 23DMI have been calculated with TD-DFT at the B3LYP/6-31G(d,p) level of theory. For both the DMIs the calculated energy of the HOMO is nearly −4.68 eV and that of the LUMO is 0.01 eV, giving an energy gap of 4.69 eV. Thus, HOMO–LUMO gap is nearly equal to the value of ^1L_b vertical transition energy ∼4.71 eV (Table 2).

Excited state. The vertical excitation energies and oscillator strengths calculated in the gas phase as well as in the solvent phase with TD-DFT at the B3LYP/6-31G(d,p) level of theory are presented in Table 1, along with the experimental values in parentheses.

TD-DFT predicts that the oscillator strength of the second singlet state is greater than that of the first singlet state. From this observation, the first and the second singlet states may be assigned as ^1L_b and ^1L_a transitions, respectively for both DMIs. Thus TD-DFT correctly predicts two low lying electronic transitions: ^1L_a and ^1L_b.

Transition configurations and oscillator strengths calculated by B3LYP/6-31G(d,p) basis for ^1L_b and ^1L_a transitions for 12DMI and 23DMI are shown in Table 2. The ^1L_b band of DMI (12 or 23) is characterized predominantly by a HOMO–LUMO transition with to a lesser extent, a contribution from a HOMO−1 to LUMO+1 transition. Whereas for the ^1L_a band HOMO−1 to LUMO transition is dominating and HOMO to LUMO transition contributes to the lesser extent to the characterization of ^1L_a band.

All the above computed results indicate the possibility of mixing of the closely lying electronic states ^1L_a (S_2) and ^1L_b (S_1), which was apparent from the experiment.

Predicted transition energies from TD-DFT method are all within 0.5 eV of experimental values of ^1L_a and ^1L_b of both the DMIs and thus correlate well with the experimental data. TD-DFT method is less accurate for calculating the oscillator strengths of both 12DMI and 23DMI. It is yielded from TD-DFT that there is an appreciable shift in energy for singlet states in switching over from the gas phase to the solvent phase (Table 1).

Transition dipoles. The TD-DFT simulated transition dipoles of DMIs in EtOH environment for both the ^1L_b and ^1L_a transitions possess small out-of-plane contributions (0.0016 a.u. and 0.0067 a.u. for 12DMI and 0.0007 a.u. and 0.0001 a.u. for 23DMI). As the out-of-plane contributions are nearly negligible, DMIs could be treated as planar molecules. Photophysical and spectroscopic properties of DMIs are found to be very similar to the corresponding properties of planar indole and monosubstituted indoles. Thus, in case of nearly planar aromatics DMIs, the electronic transitions between π and π^* orbitals (π–π^* transitions) are symmetric with respect to the molecular plane.

In the solvent EtOH, the TD-DFT calculation yielded a value of ∼58° for the angle between the transition dipole moments ^1L_a and ^1L_b for both 12DMI and 23 DMI. As most of the organic compounds possesses these two transition (^1L_b and ^1L_a) which are generally orthogonal (angle between them is ∼90°) to each other, these results of much smaller angle between the two transitions of the present DMIs are indicative of a fair chance of

Table 1
TD-DFT simulation of vertical excitation energies and oscillator strengths of DMI at the B3LYP/6-31G(d,p)

Name of the molecule	Orbitals	Energy (eV)					Oscillator strength (a.u.)		
		Gas phase	EtOH (expt.)	ΔE (cm^{-1})	ACN (expt.)	ΔE (cm^{-1})	Gas phase	EtOH (expt.)	ACN (expt.)
12DMI	^1L_b	4.7096	4.6577 (4.261)	3618	4.67 (4.246)	3739	0.0154	0.0143 (0.068)	0.0146 (0.0604)
	^1L_a	4.8868	4.8766 (4.397)	3950	4.8824 (4.381)	4079	0.0814	0.056 (0.2075)	0.062 (0.1044)
23DMI	^1L_b	4.7076	4.6776 (4.2606)	2908	4.6566 (4.2665)	3558	0.0146	0.014 (0.0488)	0.0139 (0.0803)
	^1L_a	4.8973	5.0101 (4.3811)	4163	4.8899 (4.3873)	4113	0.056	0.035 (0.0881)	0.038 (0.0875)

The oscillator strengths were measured from the absorption spectra by using the equation $f = 4.32 \times 10^{-9} \int \varepsilon(\upsilon)\, d\upsilon$.

Table 2
Transition configurations from B3LYP/6-31G(d,p) for the ground ^1L_a and ^1L_b states

Name of the molecule	Orbitals	Configuration	Coefficient	Energy (eV)	Oscillator strength (a.u.)
12DMI	^1L_b	HOMO–LUMO	0.58060	4.7096	0.0154
		(HOMO−1)–(LUMO+1)	0.16805	4.7096	0.0154
	^1L_a	(HOMO−1)–LUMO	0.51872	4.8868	0.081
		HOMO–LUMO	0.16552	4.8868	0.081
23DMI	^1L_b	HOMO–LUMO	0.59547	4.7076	0.0146
		(HOMO−1)–(LUMO+1)	0.16146	4.7076	0.0146
	^1L_a	(HOMO−1)–LUMO	0.53936	4.8973	0.056
		HOMO–(LUMO+1)	−0.43939	4.8973	0.056

mixing of the two lowest lying electronic states ^1L_a and ^1L_b. This proposition is in well agreement with the experimental findings made from the steady state polarization measurements as discussed in Section 3.1.1.

3.1.2. Changes in the nature of UV–vis spectra of DMIs in presence of well-known electron acceptor TCNQ

From the UV–vis spectrum, it is apparent that TCNQ absorbs at around 400 nm with a shoulder at 375 nm position in ACN (inset in Fig. 2). Though 12DMI and 23DMI do not exhibit any absorption band beyond 300 nm, but in presence of TCNQ a broad charge transfer (CT) band at around 470 nm region along with the formations of the three groups of new bands with λ_{max} of 685 nm, 749 nm and 848 nm was observed (Fig. 4), whatever be the polarity of the medium, highly polar ACN ($\varepsilon_s \sim 37.5$) or relatively less THF ($\varepsilon_s \sim 7.6$). Comparing the absorption profile of the three new group of the absorption bands with that Li^+ $TCNQ^-$, it could be inferred that these bands are due to $TCNQ^-$ anionic species [19].

However, the stability of the bands in the two different solvents ACN and THF appears to be different. In ACN, the three groups of bands of anionic species of TCNQ along with the CT band at 470 nm region were found to grow with time (Fig. 4a). The observation indicates that the formation of $TCNQ^-$ anions which might result from the intermolecular charge transfer interactions between DMIs and TCNQ proceeded through direct interaction between these two redox partners and not through the complex formation. Both the simultaneous augmentation of CT and anionic bands reveal that the ground state electron transfer reactions between the electron donor DMI and acceptor TCNQ is very slow in ACN medium.

In less polar THF solvent, the situation becomes somewhat different. Though the $TCNQ^-$ anionic absorption bands of similar nature, as observed in ACN medium, develops within 600–900 nm domain but their intensities slowly diminished with time (Fig. 4b), contrary to the observation made in ACN. Nevertheless, the significant augmentation of CT absorption band peaking at 470 nm was found. Thus in THF the ground state CT band becomes gradually stable with time. It is possible that due to the close proximity of the anions and cationic species within contact ion-pair, which is generally formed in non-polar ($\varepsilon_s \sim 2$) or less polar ($\varepsilon_s \sim 7$) media, CT or ion-pair band formation may facilitate rather than formations of free or solvent separated ions. Though some free or solvent separated ions (both $TCNQ^-$ anions and indolyl cations) are formed during the process should gradually disappear with time due to lack of productions of further ions. However, to present clear-cut mechanisms of the above observations, further investigations on the similar systems seem to be necessary. In presence of TCNQ, similar type of observation of formations of both CT band and TCNQ anions from the interactions between stilbenes and TCNQ has been reported previously by Jin et al. [19].

3.1.3. Changes in the fluorescence emission spectra

In highly polar ACN and less polar THF, the fluorescence intensity of a present DMI strongly quenches in presence of the electron acceptor TCNQ (Fig. 5a–d). In the quenching measurements, the concentrations of DMIs and TCNQ were chosen in such a way that at 290 nm excitation wavelength, which was used to excite the fluorescence spectra of DMIs, the quencher molecules TCNQ are transparent (inset in Fig. 5a). Thus the

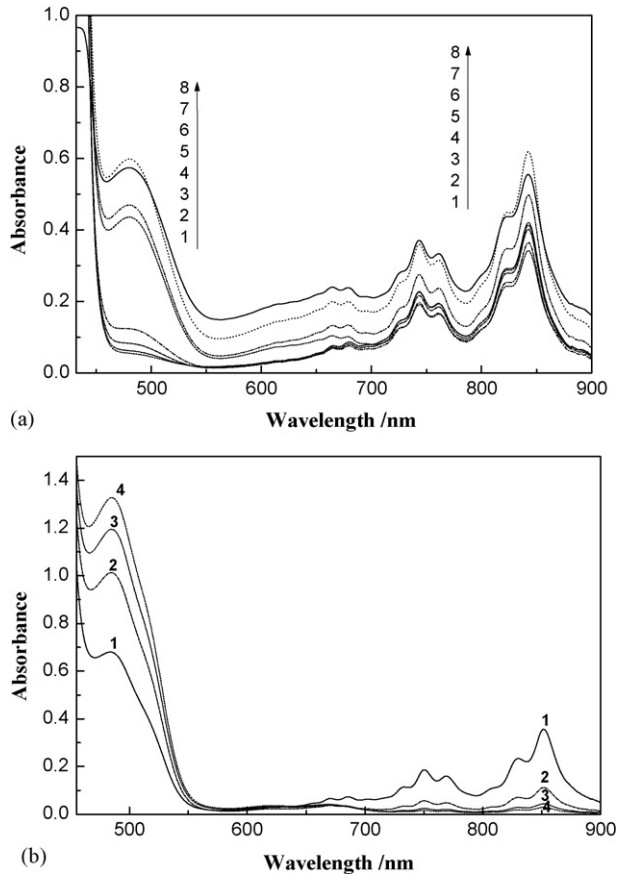

Fig. 4. (a) Time dependence of UV–vis absorption spectra of the mixture of 23DMI (2.38×10^{-4}) and TCNQ (1.88×10^{-3}) in ACN at (1) 0 min, (2) 15 min, (3) 30 min, (4) 1 h 40 min, (5) 6 h 40 min, (6) 16 h 40 min, (7) 20 h 55 min, and (8) 24 h 05 min. (b) Time dependence of UV–vis absorption spectra of the mixture of 23DMI (2.38×10^{-4}) and TCNQ (1.88×10^{-3}) in THF at (1) 0 min, (2) 1 h, (3) 2 h, and (4) 4 h 20 min.

inner-filter effect as a possible source of quenching phenomena could be ruled out.

Though the fluorescence of DMI (12 or 23) is sufficiently quenched with gradual addition of TCNQ but the quenching does not occur efficiently over the entire band envelop, 300–450 nm, of DMI fluorescence. A sufficiently weak broad fluorescence band gradually develops within 400–450 nm regime with increasing quencher concentrations. Following the observations made by earlier authors [5] this band could logically be ascribed to an exciplex emission. In the case of 23DMI relatively prominent emissive exciplex, though still very weak, was found both in ACN and THF, relative to the situation observed in case of 12DMI where very weak but a genuine band builds up at 425 nm at relatively higher quencher concentration used in the present measurements. By monitoring the 425 nm wavelength, an attempt was made to measure the fluorescence lifetime of this species. The lifetime observed was of the same order of magnitude as that of the DMI monomer itself (~8.3 ns). Thus, we were not able, unfortunately, to separate out this species from the large fluorescence band envelop of DMI by using time resolved spectroscopic technique though its presence was observable from the steady state measurements.

From Fig. 6a and b it is observed that the fluorescence quenching of the present DMIs in presence of the quencher TCNQ does not obey the simple Stern–Volmer (SV) relation [22–24]:

$$\frac{f_0}{f} = 1 + K_{SV}[Q],$$

K_{SV} ($=k_q\tau_0$) is the SV constant, k_q the bimolecular dynamic quenching rate constant and τ_0 corresponds to the fluorescence lifetime of the fluorescer DMI in the absence of a quencher (TCNQ).

f_0 and f denote the relative integrated fluorescence emission intensities of the fluorescer without and in presence of the quencher concentration [Q], respectively. It is apparent from Fig. 6a and b that the SV plots are curved upwards. The positive deviation from the linearity was observed earlier in several cases of quenching studies [25–27]. Moreover, the fluorescence lifetimes of unquenched DMIs ($\tau_0 \sim 8.4$ ns) and quenched ones (~8.3 ns) were found to be nearly (within the experimental error) the same. Thus, the steady state coupled with time resolved quenching measurements demonstrate that the quenching should be of static type quenching [28,29]. The observation of ground state CT complex, as discussed above, further confirms this proposition. However, the possibility of the concurrent occurrences of dynamic processes (photoinduced electron transfer, excitational energy transfer) along with the static mode could not be ruled out. However, relatively larger contributions from the static process may significantly mask the dynamic effect. Attempts were made next to explore the possibility of the occurrences of dynamic processes, how small its contribution may be compared to the associated static phenomena, involved within the present fluorescer–quencher systems. The experimental investigations undertaken to explore this possibility are described below.

3.1.4. Search for the possibility of occurrences of electron transfer reactions within DMIs and TCNQ

3.1.4.1. Electrochemical investigations. The half-wave oxidation potentials, $E^{OX}_{1/2}(D/D^+)$ of 12DMI and 23DMI and the half-wave reduction potential $E^{RED}_{1/2}(A^-/A)$ of TCNQ were measured by using cyclic voltammetry, the details of which are given in the experimental section. The redox potential values are shown in Table 3. The observed values indicate that the present DMIs act as electron donors in presence of TCNQ, which serves as the acceptor in photoinduced electron transfer (PET) reactions. The Gibb's free energy (ΔG°_{ET}) of electron transfer (ET) reactions was computed from the well known Rehm–Weller relation [5,30–32]:

$$\Delta G^\circ_{ET} = E^{OX}_{1/2}(D/D^+) - E^{RED}_{1/2}(A^-/A) - E^*_{0,0}$$

(neglecting the coulomb stabilization term as its contribution to the ΔG°_{ET} value in ACN is very small, ~ 0.06 eV)

$E^*_{0,0}$ is the first singlet–singlet transition energy (0, 0 band).

From Table 3, it appears that there is a possibility of occurrence of highly exergonic ($-\Delta G^\circ_{ET} \geq 2.0$ eV) PET reactions

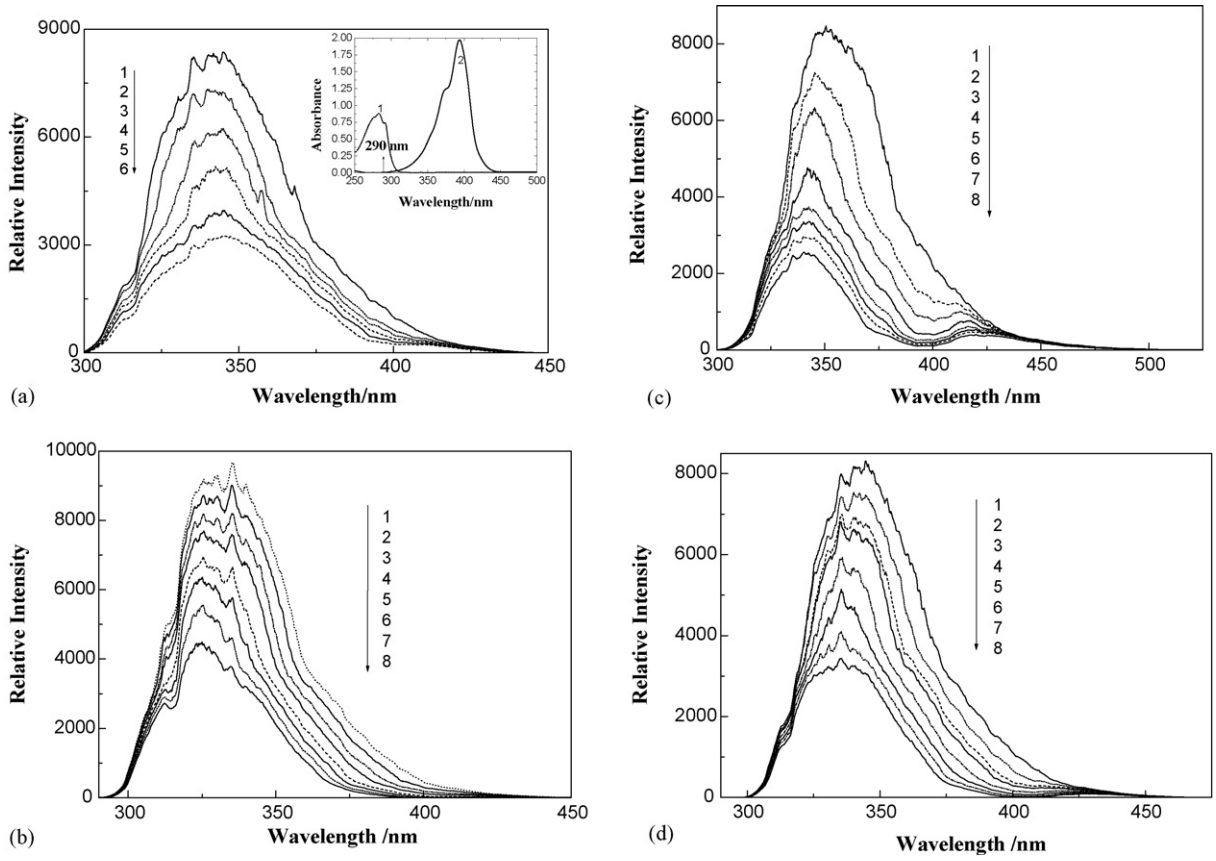

Fig. 5. (a) Fluorescence emission spectra of 12DMI in ACN (concentration $\sim 1.18 \times 10^{-4}$ mol dm^{-3}) ($\lambda_{ex} = 290$ nm) in the presence of TCNQ of concentration (mol dm^{-3}) in (1) 0, (2) 6.48×10^{-6}, (3) 1.29×10^{-5}, (4) 1.91×10^{-5}, (5) 2.53×10^{-5}, and (6) 3.14×10^{-5}. Inset: UV–vis absorption spectra of 12DMI (concentration $\sim 1.18 \times 10^{-4}$ mol dm^{-3}) and TCNQ (concentration $\sim 3.14 \times 10^{-5}$ mol dm^{-3}) in ACN at 296 K. (b) Fluorescence emission spectra of 12DMI in THF (concentration $\sim 1.22 \times 10^{-4}$ mol dm^{-3}) ($\lambda_{ex} = 290$ nm) in the presence of TCNQ of concentration (mol dm^{-3}) in (1) 0, (2) 6.48×10^{-6}, (3) 1.29×10^{-5}, (4) 1.91×10^{-5}, (5) 2.53×10^{-5}, (6) 3.14×10^{-5}, (7) 3.74×10^{-5}, and (8) 4.33×10^{-5}. (c) Fluorescence emission spectra of 23DMI in ACN (concentration $\sim 1.22 \times 10^{-4}$ mol dm^{-3}) ($\lambda_{ex} = 290$ nm) in the presence of TCNQ of concentration (mol dm^{-3}) in (1) 0, (2) 6.48×10^{-6}, (3) 1.29×10^{-5}, (4) 1.91×10^{-5}, (5) 2.53×10^{-5}, (6) 3.14×10^{-5}, (7) 3.74×10^{-5}, and (8) 4.33×10^{-5}. (d) Fluorescence emission spectra of 23DMI in THF (concentration $\sim 1.22 \times 10^{-4}$ mol dm^{-3}) ($\lambda_{ex} = 290$ nm) in the presence of TCNQ of concentration (mol dm^{-3}) in (1) 0, (2) 6.48×10^{-6}, (3) 1.29×10^{-5}, (4) 1.91×10^{-5}, (5) 2.53×10^{-5}, (6) 3.14×10^{-5}, (7) 3.74×10^{-5}, and (8) 4.33×10^{-5}.

from the thermodynamic point of view between the excited (S1) DMI and ground TCNQ. Even when the acceptor TCNQ be excited, it undergoes relatively less exergonic ($-\Delta G^{\circ}_{ET} \sim -2$ eV in case of 12DMI and -1.85 eV for 23DMI) PET reactions with the ground state donor molecules DMI. On the other hand the low positive values of ΔG°_{ET} observed when both the donor and acceptor moieties are in the ground state demonstrate the occurrence of charge separation reactions in low endergonic region. From the above experimental measurements and theoretical computations it seemingly indicates that when either of the reacting species (redox center) is excited, highly exergonic PET reactions occur, possibly in the Marcus inverted region where slow reaction rate, less than diffusion controlled, could be expected.

Table 3
Redox potentials of the reactive sites and Gibbs free energies (ΔG°_{ET}) associated with photoinduced ET reactions in ACN fluid solutions at 296 K (* denotes the excited singlet, $(T)^*$ signifies the excited triplet state)

System	$E^{OX}_{1/2}(D/D^+)$ (V)	$E^{RED}_{1/2}(A^-/A)$ (V)	$E^*_{0,0}$ (eV)	ΔG°_{ET} (eV)
$12DMI^*$+TCNQ + ACN	+0.68	−0.35	4.28	−3.25
$23DMI^*$+TCNQ + ACN	+0.90	−0.35	4.28	−3.03
12DMI + TCNQ + ACN	+0.68	−0.35		+1.03
23DMI + TCNQ + ACN	+0.90	−0.35		+1.25
12DMI + $TCNQ^*$ + ACN	+0.68	−0.35	3.10	−2.07
23DMI + $TCNQ^*$ + ACN	+0.90	−0.35	3.10	−1.85
$12DMI(T)^*$ + TCNQ + ACN	+0.68	−0.35	3.09	−2.06
$23DMI(T)^*$ + TCNQ + ACN	+0.90	−0.35	3.09	−1.84

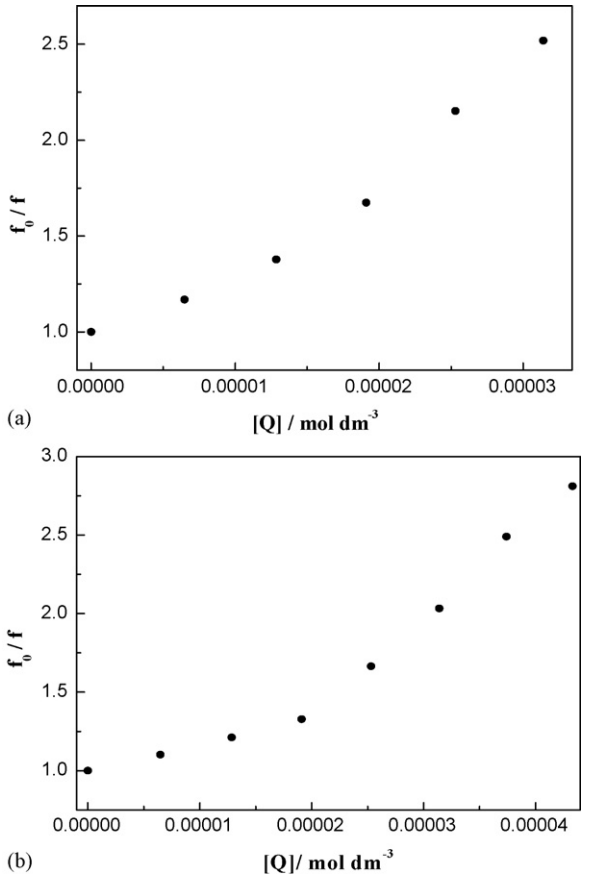

Fig. 6. (a) Stern–Volmer (SV) plot from steady state fluorescence emission intensity measurements in the case of singlet (S_1) excitation of 12DMI in the presence of TCNQ in ACN fluid solution at 296 K. (b) Stern–Volmer (SV) plot from steady state fluorescence emission intensity measurements in the case of singlet (S_1) excitation of 12DMI in the presence of TCNQ in THF fluid solution at 296 K.

3.1.4.2. Nanosecond laser flash photolysis investigation. Using the third harmonic (∼355 nm) output of the Nd:YAG laser system the transient absorption spectra of the mixture of a DMI and TCNQ were measured. Since 355 nm light could excite the TCNQ only (Fig. 1), the PET reactions should occur between excited singlet TCNQ and ground state donor DMI (12 or 23). As it is apparent from the values of $-\Delta G^{\circ}_{ET}$, which are ∼2.07 eV for ^{1}TCNQ* + 12DMI and ∼1.85 eV for ^{1}TCNQ* + 23DMI systems, the probability of occurrence of PET reactions from the thermodynamic point of view is high, it may be expected that the transient absorption spectra of anionic species, as a product of PET process, could be seen from the measurements.

The laser photolysis in ACN medium of the mixture of DMI and TCNQ yields a transient species between 350 nm and 450 nm (Fig. 7), λ_{max} being at 420 nm position. Another transient, adjacent to 420 nm band, was also found within the region of 450–500 nm peaking at about 460 nm. As it is seen from the figure, the transient absorption spectra gradually decay out with the increase of delay times between the exciting and analyzing pulses. From the kinetics of the transient absorption decay at 420 nm (shown in the inset of Fig. 7), a single species with lifetime ∼1.2 μs was obtained. As reported by earlier authors [33,34], the formation of $TCNQ^-$ anion is responsible for this

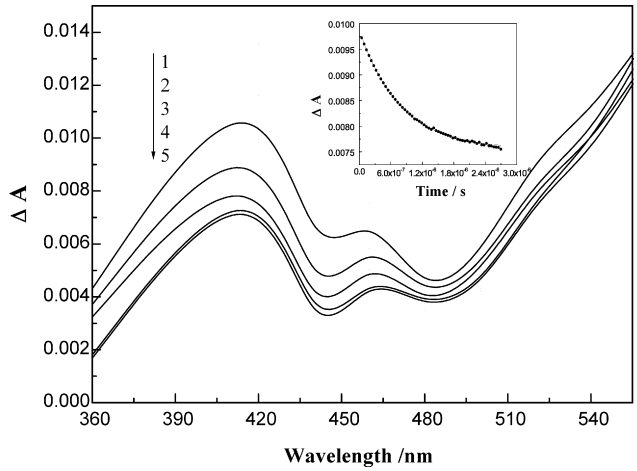

Fig. 7. Transient absorption spectra of the mixture of TCNQ and 12DMI (excitation wavelength ∼355 nm, laser pulse energy ∼6 mJ pulse^{-1}) at the ambient temperature at delay times: (1) 0.3 μs, (2) 0.8 μs, (3) 1.3 μs, (4) 3.3 μs, and (5) 3.8 μs measured in ACN. Inset: time profile of the absorbance (A) of the acceptor TCNQ radical anion in the presence of 12DMI at 420 nm (the concentrations of DMI of 2.38×10^{-3} and TCNQ of 1.88×10^{-2} in ACN have been used).

band. As the delay used is in the microsecond range, it is logical to presume that electron transfer also occurs in the triplet state through the mechanism as proposed in Scheme 1. With increase of delay in this time domain, 420 nm band decreases due to charge recombination process. Scheme 1 may be proposed from the above experimental findings, where k_{CRT} represents the rate due to the charge recombination giving rise to the excited triplets of the donor or acceptor, and k_{CRG} is the rate due to charge recombination giving rise to ground state. k_{dis} relates to the dissociation processes to form free or solvent separated anions and cationic species.

The superscripts 1 and 3 represent the excited singlet and triplet states and (*) signifies the excited state.

An attempt was made to estimate the values of Gibb's free energy changes for back electron transfer reactions by ion-pair recombination to form ground state, $\Delta G_b(G)$ and excited triplets, $\Delta G_b(T)$ of both the redox partners, by using the following expressions,

$$\Delta G_b(G) = -E^{OX}_{1/2}(D/D^+) + E^{RED}_{1/2}(A^-/A),$$

$$\Delta G_b(T) = E^{RED}_{1/2}(A^-/A) - E^{OX}_{1/2}(D/D^+) + E^*_T$$

where E^*_T is the triplet energy level.

The values $\Delta G_b(G)$ for 12DMI/TCNQ and 23DMI/TCNQ were estimated to be −1.03 eV and −1.24 eV, respectively. Both the values are negative and exergonic and thus show the possibility, from the thermodynamic point of view, of formation of ground state redox components by charge recombination mechanism in cases of DMI (both 12 and 23) and TCNQ pair.

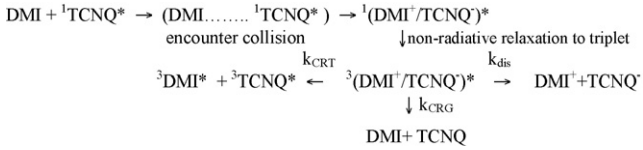

Scheme 1.

Since TCNQ molecule shows no phosphorescence, many attempts to determine the energy of its triplet state, E_T^*, have failed so far. As the triplet energy of TCNQ is not known, $\Delta G_b(T)$ could not be estimated accurately. Nevertheless, Frankevich et al. [35] determined the energy of the triplet state of TCNQ using fluorescence quenching of the weak charge-transfer complexes phenazine–TCNQ and fluorene–TCNQ in the process of fission of their excited singlet state into two triplet states. Using this procedure, they determined the energy of the triplet state of TCNQ whose value was around ~8865 cm^{-1} or 1.10 eV. Thus, from the expression of $\Delta G_b(T)$, it is apparent that its value will be around +0.07 for 12DMI/TCNQ and −0.14 eV for 23DMI/TCNQ pair. As the value of $\Delta G_b(G)$ is much more negative, i.e., more exergonic relative to the values of $\Delta G_b(T)$ for both the donor–acceptor pairs studied in the present investigation, the possibility of the formation of triplets of the redox components by recombination mechanism is very slim and may be excluded. On the other hand, the probability of formation of ground state products by ion-pair recombination seems to be rather high. This exactly what we could conclude from the transient decay analysis of 460 nm, which, as reported by Cho et al. [34] may be due to TCNQ monomeric triplet. Nevertheless, the kinetic decay analysis at 460 nm clearly shows that the lifetime is of the same order of magnitude (~1 μs) as that of the TCNQ anionic species observed at 420 nm. It may be presumed that if some triplet TCNQ be at all formed due to ion-pair recombination mechanisms, its yield may be expected to be of very low. Thus it is possible that the triplet may be hidden well within the neighboring transient absorption band of the $TCNQ^-$ anions.

The time profile of the absorption of the acceptor $TCNQ^-$ anion (inset of Fig. 7) shows that with further increase of the delay beyond 5 μs, the value of absorbance of the anion becomes constant. The ion-dissociation or charge separation yield ϕ_R is obtained [36] by taking the ratio of the constant absorbance at long delay times due to dissociated ions and the initial value estimated by extrapolating the ion absorbance to $t = 0$ in inset of Fig. 7. A large yield of the dissociated ion radical ($\phi_R \sim 0.8$) was obtained. Such large yield of charge separation was not found, as reported from our research group earlier [5], when the same donor DMI molecules undergo photoinduced electron transfer (PET) reactions with another well known electron acceptor, 9-cyanoanthracene (9CNA), though the reduction potential of the 9CNA acceptor is greater (~−1.13 V) than the presently used acceptor TCNQ (~−0.35 V). In the case of DMI–9CNA system, the value of ϕ_R obtained was only 0.15. From this observation it seemingly indicates that the rate associated with the energy wasting charge recombination (k_{CR}) process should be much smaller in the case of the presently used donor–acceptor (DMI–TCNQ) systems than the corresponding rate observed in the case of previously reported DMI–9CNA pairs. Moreover, highly exergonic ΔG_{ET}° values (≤−2 eV, Table 3), obtained when either excited donor DMI or acceptor TCNQ molecules undergo PET reactions with the ground TCNQ or DMI molecules, indicate in favor of occurrence of PET reactions in Marcus inverted region.

To corroborate further this proposition, the total nuclear reorganization energy, λ ($=\lambda_S + \lambda_V$) was computed from the expression, shown below, of the dielectric continuum model of a solvent as proposed by Marcus [37–38] (λ_S the nuclear reorganization energy originates from solvent oscillators and λ_V from oscillators within the molecule):

$$\lambda_S = \frac{e^2}{4\pi\varepsilon_0}\left(\frac{1}{\varepsilon_{op}} - \frac{1}{\varepsilon_S}\right)\left(\frac{1}{2r_d} + \frac{1}{2r_a} - \frac{1}{R}\right),$$

The estimated λ_S value was computed to be 0.7 eV assuming $R \geq 7$ Å for outer sphere reaction [39,40].

The total nuclear reorganization value, λ ($=\lambda_S + \lambda_V$) was estimated to be about ~1.0 eV for the present DMI–TCNQ system [λ_V value was assumed to be ~0.3 eV, which is the characteristic value of aromatic D–A system [36]].

The observation of $-\Delta G_{ET}^{\circ} > \lambda$ further confirms that the PET reactions in the present investigation fall in the Marcus inverted region. As in the Marcus inverted region, slow rate of charge recombination occurs, the observation of large yield (~0.8) of charge-separated species is in accord to our expectation.

From the moderate value of λ (~1.0 eV) and the observed large charge separation yield, $\phi_R \sim 0.8$, resulted from the highly exergonic PET reactions in Marcus inverted region, it may be presumed that building up of artificial or model photosynthetic systems with the present donor 12DMI or 23DMI and well known electron acceptor TCNQ system could be possible. Using various flexible or semi-rigid and rigid olefinic spacers between the DMI and TCNQ, synthesis of several dyad systems are underway.

4. Concluding remarks

Though Stern–Volmer analysis alone was found to be unable to provide information of the concurrent occurrences of dynamic processes like photoinduced electron transfer with static quenching but electrochemical measurements coupled with time resolved spectroscopic investigations reveal that TCNQ could act as a potential electron acceptor molecule with the donors DMI to undergo highly exergonic ($-\Delta G_{ET}^{\circ} \geq 2$ eV) photoinduced electron transfer reactions in Marcus inverted region (mir). Moreover, observation of large yield ($\phi_R \sim 0.8$) of charge-separated species, as obtained from the transient absorption decay analysis, along with $-\Delta G_{ET}^{\circ} > \lambda$ is indicative of the presence of mir where the energy wasting charge recombination processes play minor role within the DMI–TCNQ systems. As the value of nuclear reorganization energy, λ is relatively low (~1.0 eV) for the present donor–acceptor pairs in comparison to the corresponding values observed in case of other organic electron donor/TCNQ systems, efficient photoconductors could possibly be developed by using DMI and TCNQ. It is anticipated that the present donor and acceptor (DMI and TCNQ) molecular systems being connected by suitable spacers may undergo intramolecular charge transfer upon excitation and display photoconducting and non-linear optical properties. Synthesis of such organic systems is underway.

Supporting information available

B3LYP/6-31G(d) optimized geometry of 12DMI and 23DMI in the gas phase. This material is available free of charge via the internet at http://pubs.acs.org.

Acknowledgments

The authors are grateful to Dr. S. Ghosh of the Department of Chemistry, Presidency College, Kolkata for extending his facility to measure fluorescence lifetimes. We wish to express our heartiest thanks to Prof. Samita Basu of Saha Institute of Nuclear Physics, Kolkata, for helping in the measurements of the transient absorption spectra by laser Flash photolysis technique. We are also thankful to Mr. S. Karan and Mr. J. Sarkar for their helpful cooperation in the calculations. TG gratefully acknowledges the financial assistances provided by the Council of Scientific and Industrial Research (CSIR), New Delhi, India in the form of grants (Project No. 01 (1883)/03/EMR-II).

References

[1] E. Prasad, K.R. Gopidas, J. Am. Chem. Soc. 123 (2000) 1159.
[2] L.D. Book, D.C. Arnett, H. Hu, N.F. Scherer, J. Phys. Chem. A 102 (1998) 4350.
[3] S.R. Greenfield, M. Seihert, M.R. Govindjee, Wasielewski, Chem. Phys. 210 (1995) 279.
[4] A. Weedon, D.H. Volman, G. von Bünau, U.S. Wiely, D.C. Neckers (Eds.), Advances in Photochemistry, Vol. 22, J. Wiley & Sons, 1997.
[5] S.K. Pal, T. Bhattacharya, T. Misra, R.D. Saini, T. Ganguly, J. Phys. Chem. A 107 (2003) 10243.
[6] T. Misra, A.K. De, S.K. Pal, T. Bhattacharya, T. Ganguly, Proc. Indian Acad. Sci. (Chem. Sci.) 114 (2002) 547.
[7] C. Ho, S.J. Slater, C.D. Stubbs, J. Photochem. Photobiol. A: Chem. 142 (2001) 163.
[8] A.L. Sobolewski, W. Domcke, Chem. Phys. Lett. 315 (1999) 293.
[9] M. Gil, J. Marczyk, S. Dobrin, P. Kaaszynski, J. Waluk, J. Mol. Struct. 475 (1999) 141.
[10] A.I. Novaira, C.D. Borsarelli, J.J. Cosa, Previtali, J. Photochem. Photobiol. A: Chem. 115 (1998) 43.
[11] P. Jennings, A.C. Jones, A.R. Mount, A.D. Thomson, J. Chem. Soc. Faraday Trans. 93 (1997) 3791.
[12] A.R. Mount, Res. Chem. Kinet. 4 (1997) 1.
[13] S. Dobrin, P. Kaszynski, A. Starkhin, J. Waluk, Chem. Phys. 216 (1997) 179.
[14] S. Itoh, N. Takada, T. Ando, S. Haranou, X. Huang, Y. Uenoyama, Y. Ohshiro, M. Komatsu, S. Fukuzumi, J. Org. Chem. 62 (1997) 5898.
[15] S. Nigam, R.S. Sarpal, M. Belletete, G. Durocher, J. Colloid Interf. Sci. 177 (1996) 143.
[16] R.S. Sarpal, M. Belletete, G. Durocher, J. Photochem. Photobiol. A: Chem. 86 (1995) 201.
[17] J.G. Mackintosh, C.R. Redpath, A.C. Jones, P.R.R. Langridge-Smith, D. Reed, A.R. Mount, J. Electroanal. Chem. 375 (1994) 163.
[18] J.G. Macintosh, A.R. Mount, J. Chem. Soc. Faraday Trans. 90 (1994) 1121.
[19] J. Jin, J.S. Kim, J.D. Kim, Bull. Korean Chem. Soc. 9 (1988) 167.
[20] S.K. Pal, S.K. Batabyal, T. Ganguly, Chem. Phys. Lett. 406 (2005) 420.
[21] S.K. Pal, T. Sahu, T. Misra, P.K. Mallick, M.N. Paddon-Row, T. Ganguly, J. Phys. Chem. A 108 (2004) 10395.
[22] O. Stern, M. Volmer, Phys. Z. 20 (1919) 183.
[23] P.R. Bevington, Data Reduction Error Analysis for the Physical Sciences, McGraw-Hill, New York, 1969.
[24] M. Maiti, T. Misra, S. Sinha, S.K. Pal, D. Mukherjee, R.D. Saini, T. Ganguly, J. Lumin. 93 (2001) 261.
[25] T. Sahu, S.K. Pal, T. Misra, T. Ganguly, J. Photochem. Photobiol. A: Chem. 171 (2005) 39.
[26] M.C. Rath, H. Pal, T. Mukherjee, J. Phys. Chem. A 105 (2001) 7945.
[27] M.R. Eftink, C.A. Ghiron, J. Phys. Chem. 80 (1976) 486.
[28] J.B. Birks, Photophysics of Aromatic Molecules, Wiley, New York, 1970, p. 443.
[29] K.K. Rohatgi-Mukherjee, Fundamentals of Photochemistry, Wiley Eastern Limited, New Delhi, 1986.
[30] D. Rehm, A. Weller Sr., J. Chem. 8 (1970) 259.
[31] D. Rehm, A. Weller, Ber. Bunsen-Ges. Phys. Chem. 73 (1969) 837.
[32] S. Sinha, R. De, T. Ganguly, Spectrochim. Acta A 54 (1998) 145.
[33] A.K. Jana, S.K. Mukhopadhya, B.B. Bhowmik, Spectrochim. Acta A 57 (2001) 2687, and references therein.
[34] K.S. Cho, Y. Nam, D. Kim, W.H. Lee, J. Choi, Synth. Metals 129 (2002) 157.
[35] E.L. Frankevich, A.N. Chaban, M.M. Triebel, J.U. von Schütz, H.C. Wolf, Chem. Phys. Lett. 177 (1991) 283.
[36] T. Ganguly, D.K. Sharma, S. Gauthier, D. Gravel, G. Durocher, J. Phys. Chem. 96 (1992) 3757.
[37] R.A. Marcus, J. Chem. Phys. 24 (1956) 966.
[38] R.A. Marcus, J. Chem. Phys. 26 (1957) 867.
[39] K. Kikuchi, J. Photochem. Photobiol. A: Chem. 65 (1992) 149.
[40] S. Sinha, R. De, T. Ganguly, J. Phys. Chem. 101 (1997) 2852.